SPINE RESEARCH

OPEN

Targeting neutrophil extracellular traps with a biomimetic patch to inhibit epidural fibrosis

Changdong Cui[a], Kun Xi[a], Jincheng Tang[a], Jie Meng[a], Feng Cai[a], Yong Gu[a] Liang Chen[a,*]

Abstract

Background: Epidural fibrosis, a major contributor to failed back surgery syndrome, involves post-operative scar adhesion and nerve compression leading to persistent pain and compromised outcomes. While neutrophil extracellular traps (NETs) are implicated in pathological scar formation, effective and sustained strategies to modulate their activity are lacking. This study aimed to leverage the anti-NETs potential of curcumin, overcoming its inherent limitations of poor bioavailability, for the active prevention of epidural fibrosis.

Methods: Curcumin (Cur) was encapsulated within core–shell poly (L-lactic acid) micro-sol electrospun fibers (MS@Cur) to enable localized, sustained delivery. The release profile and physicochemical properties of the fabricated membranes were characterized. *In vitro* studies evaluated their cytocompatibility and their ability to inhibit NETs formation by neutrophils. Efficacy was further evaluated in a rat laminectomy model, where the impact of MS@Cur implantation on NETs markers (myeloperoxidase and citrullinated histone H3), collagen deposition, and myofibroblast activation was analyzed histologically.

Results: The MS@Cur membranes demonstrated successful curcumin encapsulation, mitigating burst release and achieving sustained release for over 28 days. They showed favorable cytocompatibility and effectively inhibited NETs formation *in vitro*. *In vivo*, implantation of MS@Cur led to a notable downregulation of NETs markers. Histological analyses confirmed a significant reduction in excessive collagen deposition and aberrant myofibroblast activation at the laminectomy site.

Conclusion: The developed biomimetic dural patch enables sustained and efficient local delivery of curcumin, effectively modulating NETs formation after laminectomy. This strategy represents a novel and effective therapeutic approach for the active prevention of epidural scar formation following dural injury, with significant translational potential.

Abbreviations: α-SMA = α-smooth muscle actin, Cur = curcumin, FBSS = failed back surgery syndrome, H3cit = citrullinated histone H3, H&E = hematoxylin–eosin, MPO = myeloperoxidase, MRI = magnetic resonance imaging, NETs = neutrophil extracellular traps, PBS = phosphate buffered saline, PLLA = poly (L-lactic acid), ROS = reactive oxygen species, SEM = scanning electron microscopy

Keywords : curcumin, laminectomy, electrospinning, epidural fibrosis, neutrophil extracellular traps

1. Introduction

Failed back surgery syndrome (FBSS) remains one of the most challenging postoperative complications that compromise long-term outcomes after spinal surgery, with an incidence ranging from 10% to 40% and limited effective therapeutic options.[1–3] Among the multifactorial causes of FBSS, pathological epidural fibrosis—characterized by scar adhesion and compression of the spinal nerve roots—is widely recognized as the predominant pathological basis for persistent low back and radicular pain.[4–6] In addition, extensive scar formation and distortion of local anatomical structures significantly increase the difficulty and risk of revision surgery, posing a major challenge for clinical management.[7–9] Given the steadily increasing global incidence of lumbar degenerative disorders, effective prevention of epidural fibrosis and FBSS has become an urgent clinical need.

Following spinal decompression surgery, the host immune system is rapidly activated, recruiting large numbers of inflammatory cells such as neutrophils and macrophages to the surgical site.[7,10,11] As key effectors of innate immunity, neutrophils respond to proinflammatory cytokines (e.g., TNF-α and IL-8) and immune complexes by activating nicotinamide adenine dinucleotide

[a] Department of Orthopedics, First Affiliated Hospital of Soochow University, Orthopedic Institute, Soochow University, Suzhou, Jiangsu, China.

* Correspondence: Liang Chen, Department of Orthopedics, First Affiliated Hospital of Soochow University, Orthopedic Institute, Soochow University, 899 Pinghai Road, Suzhou 215006, China (e-mail: chenliang1972@sina.com).

Spine Research (2026) 2:1;45–57

Received: 27 October 2025 / Accepted: 15 January 2026

Published online 23 March 2026

http://dx.doi.org/10.1097/br9.0000000000000026

phosphate oxidase and enhancing mitochondrial respiration, leading to excessive production of reactive oxygen species (ROS).[12–14] The elevated ROS levels promote nuclear translocation of myeloperoxidase (MPO) and neutrophil elastase, resulting in chromatin decondensation and increased permeability of the nuclear and plasma membranes.[15,16] Consequently, nuclear DNA and intracellular components are released into the extracellular space, forming neutrophil extracellular traps (NETs)—a web-like structure composed of DNA, histones, and proteases.[13,17,18] Although NETs play a protective role in capturing and killing pathogens, their excessive formation at the laminectomy site can perpetuate inflammation, aberrantly activate fibroblasts into myofibroblasts, and stimulate excessive secretion of extracellular matrix components such as collagen. This cascade ultimately leads to pathological scar formation, impairing dural repair and functional recovery.[2,13,19] Therefore, targeted modulation of NETs formation represents a promising therapeutic strategy to prevent epidural fibrosis after spinal surgery.

Curcumin, a natural polyphenolic compound extracted from the rhizomes of *Curcuma longa*, possesses a unique bis-α, β-unsaturated diketone structure.[20,21] Owing to its potent anti-inflammatory and antioxidant properties, curcumin can effectively suppress inflammation, scavenge excessive ROS, and protect cellular integrity and function.[22–24] It has shown broad therapeutic potential in neurological and cardiovascular disorders.[25–27] More recently, curcumin has been reported to effectively inhibit NETs formation,[28–30] suggesting its promise as a candidate for mitigating excessive NETs activity in epidural fibrosis. However, the critical window for epidural scar formation extends to approximately 2 weeks postsurgery, whereas curcumin's clinical efficacy is hindered by its low bioavailability and short half-life, limiting its sustained therapeutic performance. Enhancing the release stability and bioavailability of curcumin is therefore crucial for clinical translation.[31–33] Our previous work developed a microsol electrospinning technique capable of fabricating porous, high-surface area core–shell nanofibrous membranes.[4] This technique provides significant advantages in preserving drug activity, enabling controlled release, and improving delivery efficiency and bioavailability. The core–shell architecture allows the encapsulated drug to be released in a sustained and localized manner while maintaining structural integrity and minimizing initial burst release.

Based on the potent anti-NETs potential of curcumin and the controlled-release advantages of microsol electrospinning, this study aimed to construct a biomimetic dural substitute in which curcumin is encapsulated within the core layer, while the shell provides mechanical stability and protects it from burst release in the post-laminectomy microenvironment. The objective was to modulate NETs formation and suppress pathological epidural fibrosis. Through systematic physicochemical characterization, *in vitro* assays, and *in vivo* validation in a rat dural injury model, we demonstrated that this biomimetic patch effectively delivers curcumin in a sustained manner, maintains a proregenerative microenvironment, and inhibits epidural fibrosis. This study not only provides new mechanistic insights into the prevention of epidural fibrosis but

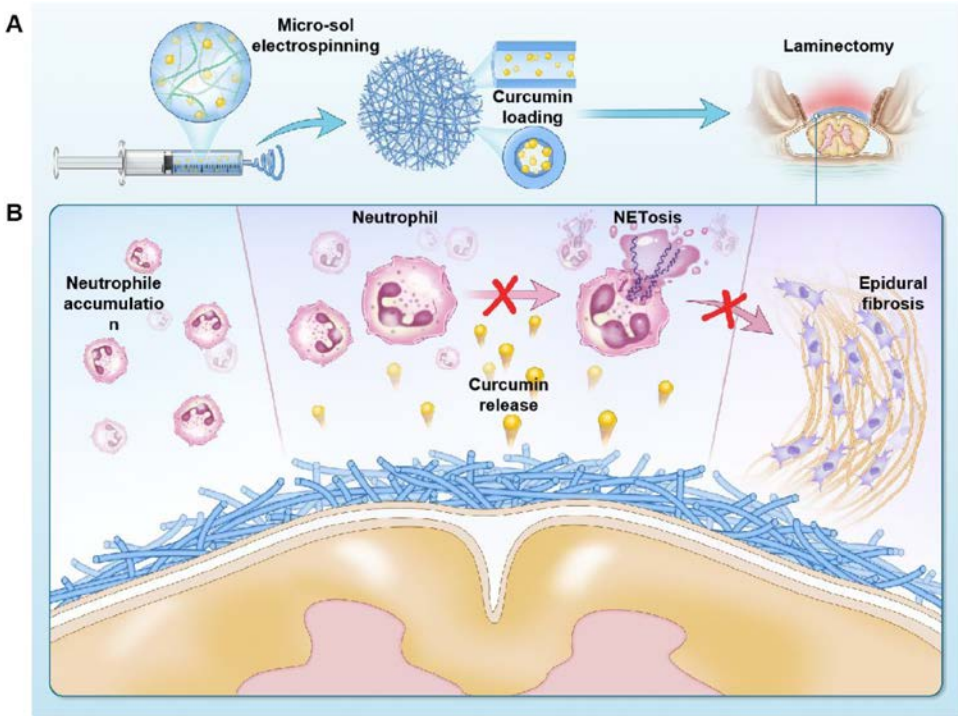

Figure 1. Construction and function of the bionic patch. (A) Schematic diagram illustrating the fabrication of the bionic patch via micro-sol-assisted electrospinning for curcumin loading. (B) Mechanism by which the bionic patch inhibits epidural fibrosis by controlling curcumin release and suppressing NETs formation. NETs = neutrophil extracellular traps.

also offers a theoretical and material basis for the development of next-generation dural biomaterials with translational potential (Fig. 1).

2. Methods and materials

2.1. Preparation of biomimetic dural patch

For the preparation of a traditional poly (L-lactic acid) (PLLA) electrospun dural patch, 0.5 g of PLLA (Ruixi, China) was dissolved in 4 g of dichloromethane under constant stirring at room temperature to form a homogeneous solution, followed by the addition of 2 g of N,N-dimethylformamide (Aladdin, China). Curcumin was first dissolved in ethanol to obtain a concentration of 2.5 $mg \cdot mL^{-1}$. The curcumin/ethanol solution was then added into the PLLA solution to achieve a final curcumin concentration of 50 $\mu g \cdot mL^{-1}$ in the electrospinning precursor. The resulting transparent and uniform solution was used for dural patch fabrication. The electrospinning was conducted using a 10-mL syringe at a feeding rate of 70 $\mu L \cdot min^{-1}$, an applied voltage of 15 kV to 18 kV, and a needle-to-collector distance of 15 cm. The nanofibrous mats were collected on an 8-cm diameter cylindrical collector covered with aluminum foil.

For the preparation of the curcumin-loaded microsol electrospun patch, 0.1 g of hyaluronic acid (HA) was dissolved in 9.9 g of deionized water to prepare a 1-wt% HA solution as the microsol core. Then, 10 µL of a 30-$mg \cdot mL^{-1}$ curcumin/ethanol solution was added to 50 µL of HA solution. Subsequently, 0.01 g of Span-80 (Sigma, USA) and 4 g of dichloromethane were introduced, followed by ultrasonic emulsification in an ice bath for 20 min to obtain a uniform milky emulsion containing curcumin microsols. Then, 0.5 g of PLLA and 2 g of N,N-dimethylformamide were added and stirred at room temperature to prepare the microsol electrospinning precursor solution, with a final curcumin concentration of 50 $\mu g \cdot mL^{-1}$. The electrospinning parameters were consistent with those of the traditional PLLA group. The resulting curcumin-loaded microsol electrospun dural substitute was denoted as MS@Cur.

2.2. Characterization of biomimetic dural patch

The microstructures of PLLA and MS@Cur electrospun membranes were observed using scanning electron microscopy (SEM; Hitachi, Japan) and transmission electron microscope (TEM; Hitachi, Japan). Prior to SEM observation, samples were sputter-coated with gold for 60 s and imaged at an accelerating voltage of 10 kV. Fiber diameter and morphology distributions were quantified from SEM images using ImageJ software.

For the measurement of Young modulus, both PLLA and MS@Cur electrospun mats were prepared as fiber strips (10.0 mm × 3.0 mm × 0.2 mm) and subjected to uniaxial tensile testing using a universal testing machine (Hengyi, China) at a crosshead speed of 2.5 $mm \cdot min^{-1}$. The stress–strain curves were recorded, and the Young modulus values were calculated from the linear region of the curves.

For degradation assays, the membranes were immersed in 30 mL of phosphate buffered saline (PBS) at room temperature, with PBS refreshed daily. At predetermined time points, samples were freeze-dried and weighed. The degradation rate was calculated as the ratio of residual weight (Wt) to the initial weight (W0), and degradation profiles were plotted accordingly.

For curcumin release analysis, 10 mg of each electrospun membrane (PLLA or MS@Cur, containing approximately 6 ng of curcumin) was immersed in 10 mL of PBS and incubated at 37 °C under shaking (120 rpm). Supernatants were collected at predetermined time intervals over 28 days, replaced with fresh PBS, and analyzed spectrophotometrically at 425 nm. A standard curve of curcumin in PBS was used to determine the released curcumin concentration at each time point, from which cumulative release profiles were generated.

2.3. Cytocompatibility of biomimetic dural patch

The cytocompatibility of PLLA and MS@Cur dural substitutes was evaluated by live/dead staining and Cell Counting Kit-8 (CCK-8) assay. Bone marrow mesenchymal stem cells were seeded onto each membrane placed in 24-well plates with the density of 1×10^4 cells/well and cultured for 3 days. Cells were stained with Live/Dead Cell Imaging Kit (Thermo Fisher Scientific, USA) at room temperature for 30 min in the dark. After rinsing, fluorescence images were obtained using a fluorescence microscope (Zeiss, Germany), and live cell counts were quantified using ImageJ. Cells cultured without scaffolds served as controls.

For the CCK-8 assay, bone marrow mesenchymal stem cells were seeded as above and cocultured for 3 and 5 days. At each time point, the culture medium was replaced with CCK-8 working solution (10% CCK-8 reagent in medium) and incubated for 4 h at 37 °C. Subsequently, 100 µL of supernatant was transferred to 96-well plates, and absorbance was measured at 450 nm using a microplate reader (BioTek, USA).

2.4. Detection of NETs formation

Neutrophils were isolated from 6- to 8-week-old C57 mice using a mouse bone marrow 647 neutrophil isolation kit (Solarbio). After erythrocyte lysis and counting, 5×10^5 cells/well of neutrophils were seeded in 24-well plates containing PLLA or MS@Cur, with blank wells as controls, and cultured in RPMI-1640 medium supplemented with 100 nM PMA (Sigma). After coculture for 3 h, SYTOX Green staining (Beyotime, China) was performed according to the manufacturer's instructions. Following PBS washing, 200 µL of working dye solution was added, and cells were incubated at 37 °C for 20 min. Samples were then washed twice with serum-free medium and imaged under an inverted fluorescence microscope.

For SEM imaging, after 3 h of coculture, cells were fixed with 4% paraformaldehyde, dehydrated through a graded ethanol series, and dried using a critical point dryer. Samples were sputter-coated with gold for 75 s and imaged at 10 kV using SEM (Hitachi, Japan).

2.5. Detection of NETs markers

For immunofluorescence staining, neutrophils were extracted and cocultured with PLLA or MS@Cur membranes as described earlier. After 3 h of co-culture, cells were washed with PBS and fixed with 4% paraformaldehyde for 30 min at room temperature. After permeabilization with Triton X-100 and blocking with 5% bovine serum albumin at 4 °C overnight, primary antibodies against MPO (A2900, Abclonal) and citrullinated histone H3 (H3cit) (RM1001, Abcam) were added (1:200 dilution) and incubated overnight at 4 °C. After washing, fluorescent secondary antibodies were applied for 3 h at room temperature in the dark, followed by 4',6-diamidino-2-phenylindole nuclear staining for 3 min. Samples were mounted with antifade medium and imaged using a laser confocal microscope. Fluorescence intensity was quantified using ImageJ software.

For Western blotting, after 3 h of coculture, neutrophils were collected by trypsinization and washed with PBS. Cells were lysed in radio immunoprecipitation assay buffer containing protease and phosphatase inhibitors, followed by centrifugation (10,000–14,000 g, 5 min). The supernatant was mixed with loading buffer (1:4 ratio) and boiled for 10 min at 100 °C. Protein concentrations were quantified using a bicinchoninic acid assay. Equal amounts of protein were separated by SDS-PAGE (8%–15%) and transferred onto polyvinylidene fluoride membranes at 400 mA. After blocking with rapid blocking buffer (Beyotime, P0220) for 20 min, membranes were incubated overnight at 4 °C with primary antibodies against MPO (A2900, Abclonal) and H3cit (RM1001, Abcam). After tris buffered saline with tween 20 washing, membranes were incubated with horseradish peroxidase-conjugated secondary antibody for 2 h at room temperature. Protein bands were visualized using a chemiluminescence imaging system, and band intensities were quantified using ImageJ.

2.6. Rat laminectomy model and patch implantation

Male Sprague-Dawley (SD) rats (weighed about 300 g) were anesthetized by intraperitoneal injection of 60 mg·kg^{-1} pentobarbital sodium. After hair removal, a midline incision was made over the L4–L5 vertebrae, and paraspinal muscles were bluntly dissected to expose the laminae. The L4–L5 laminae were removed to expose the dura mater. PLLA or MS@Cur membranes were adhered over the laminectomy site, with a blank (no material) group as control. After implantation, muscles and skin were sutured in layers. Penicillin of 400,000 U was administered intramuscularly postoperatively to prevent infection.

2.7. In vivo detection of NETs

At postoperative days 3 and 7, rats were euthanized by intraperitoneal injection of excess pentobarbital sodium. The entire lumbar spine, including vertebrae, nerves, dura mater, and epidural tissues, was harvested. The lamina-deficient segment was marked with a suture for orientation. Samples were fixed in formalin, decalcified in ethylenediaminetetraacetic acid, dehydrated, and paraffin-embedded. Sections (20 μm) were prepared using a microtome (Leica, Germany). After antigen retrieval with 0.3% hydrogen peroxide and blocking with 5% bovine serum albumin, sections were incubated with MPO (A2900, Abclonal) and H3cit (RM1001, Abcam) primary antibodies overnight at 4 °C, followed by secondary antibody incubation for 1 h at room temperature. Sections were observed under a fluorescence microscope to evaluate early postoperative NETs formation at the laminectomy site.

2.8. Magnetic resonance imaging evaluation

Eight weeks after surgery, SD rats were anesthetized with 60 mg·kg^{-1} pentobarbital sodium, and MRI scans of the lumbar spine were performed using a 1.5 T GE Signa MRI device (GE, USA). Sagittal and axial T2-weighted images were acquired, and epidural fibrosis was further graded with six samples included in each group (n = 6) according to the MRI image-based scoring system which was provided as follow (Table 1).

2.9. Histological analysis

Eight weeks after surgery, rats were euthanized and samples were processed for fixation, decalcification, dehydration, and paraffin embedding. Sections were stained with hematoxylin–eosin and Masson trichrome to evaluate late-stage epidural fibrosis and adhesion formation. Based on Masson trichrome-stained images, the epidural fibrosis area was quantified using ImageJ software.

2.10. Detection of epidural fibrosis markers in vivo

Eight weeks after surgery, spine samples were harvested, fixed, decalcified, and paraffin-embedded. After antigen retrieval with 0.3% hydrogen peroxide and blocking with 5% BSA, sections were incubated with primary antibodies against α-SMA (A2235, Abclonal) and Col-I (A21059,

Table 1

MRI-based scoring criteria.[4]

Grade	Scoring criteria
0	No fibrosis scar formation
1	Scar tissue occupying > 0% to ≤ 25% area of quadrants
2	Scar tissue occupying > 25% to ≤ 50% area of quadrants
3	Scar tissue occupying > 50% to ≤ 75% area of quadrants
4	Scar tissue occupying > 75% to ≤ 100% area of quadrants

MRI = magnetic resonance imaging.

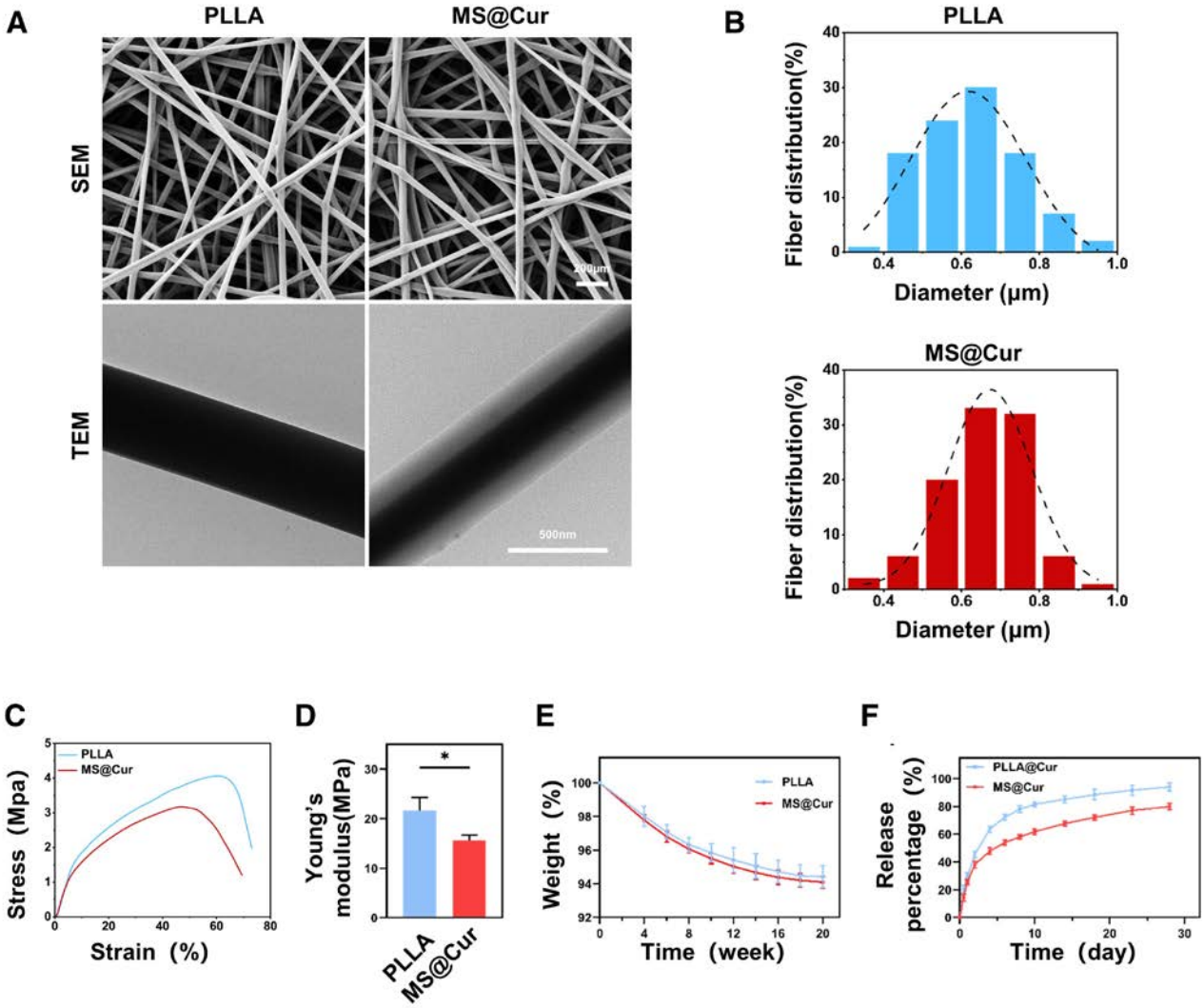

Figure 2. Characterization of the physicochemical properties of the bionic patch. (A) Representative SEM and TEM images of PLLA and MS@Cur. (B) Size distribution histograms of PLLA and MS@Cur. (C) Stress–strain curves. (D) Analysis of Young modulus. (E) *In vitro* degradation profiles. (F) Cumulative release kinetics of curcumin from PLLA and MS@Cur. $n = 3$, error bars, mean ± SD; all analyses were done using 1-way ANOVA with Tukey *post hoc* test, $^{*}p < 0.05$. ANOVA = analysis of variance, MS@Cur = curcumin-loaded microsol electrospun dural substitute, PLLA = poly (L-lactic acid), SD = standard deviation, SEM = scanning electron microscopy, TEM = transmission electron microscopy.

Abclonal) overnight at 4 °C, followed by incubation with secondary antibodies for 1 h at room temperature. Sections were imaged under an inverted microscope. The activated fibroblasts were counted on three samples from each group (n = 3). The H-Score of Col-I staining was calculated using Case viewer 2.4 software (3DHISTECH, Hungary) via method reported previously.

3. Results and discussion

3.1. Physicochemical characterization of the biomimetic dural patch

In this study, conventional electrospinning (PLLA) and microsol electrospinning (MS@Cur) techniques were employed to fabricate 2 types of fibrous membranes.[34] Their morphology, structure, mechanical properties, degradation behavior, and drug release characteristics were systematically compared to evaluate their potential in suppressing NETs formation and epidural fibrosis after laminectomy. SEM images revealed that both PLLA and MS@Cur fibers exhibited smooth surfaces, uniform structures, and homogeneous pore size distribution (Fig. 2A). TEM observations further demonstrated a distinct core–shell architecture in the MS@Cur fibers, with a dense shell layer indicating successful construction of a microsol electrospun structure capable of sustained drug release. As shown in Figure 2B, the diameter distribution analysis revealed that both PLLA and MS@Cur fibers exhibited comparable size uniformity, with MS@Cur showing slightly thicker fibers but no statistically significant difference ($P > 0.05$), suggesting that the core–shell formation did not notably affect the overall diameter distribution.

Mechanical testing showed that the MS@Cur membrane exhibited lower maximal stress before failure and a significantly reduced Young's modulus compared with conventional PLLA fibers (Fig. 2C and D), indicating decreased stiffness and increased compliance. This change may be related to the core-shell structure formed by micro-sol electrospinning and the incorporation of curcumin-containing micro-sol components, which could alter the internal fiber architecture. In spite of the declination in mechanical strength, MS@Cur maintained adequate mechanical integrity for implantation. Notably, this more compliant mechanical profile may facilitate better conformity to the laminectomy site and reduce local mechanical irritation, thereby providing a favorable structural basis for subsequent anti-NETs regulation and anti-fibrotic repair.[35] As shown in Figure 2E, MS@Cur exhibited a slightly faster degradation rate than PLLA. This behavior may be attributed to its core-shell structure, which could facilitated water infiltration into the fibers. Despite this, MS@Cur maintained good structural stability throughout the degradation period, supporting its function as a temporary physical barrier and a sustained local drug delivery platform during anti-fibrotic repair. The release profile showed that the PLLAmembrane exhibited an initial burst release of curcumin,whereas MS@Cur provided a stable and sustained releaseover 28 days with reduced initial burst, maintaining asteady drug concentration at later stages (Fig. 2F).

Collectively, these results indicate that the micro-sol electrospinning strategy successfully produced MS@Cur fibers with well-controlled morphology, adequate mechanical integrity, and a prolonged curcumin release profile. This sustained delivery can maintain therapeutic drug concentrations at the injury site, suppress the formation of NETs, block fibrosis-associated signaling cascades, and ultimately prevent epidural scar formation after laminectomy.

3.2. Cytocompatibility evaluation

Excellent cytocompatibility is a prerequisite for any tissue engineering scaffold to exert its biological therapeutic functions.[36,37] To assess the cytocompatibility of the fabricated membranes, live/dead cell staining and cell proliferation (CCK-8) assays were performed to evaluate the effects of PLLA and MS@Cur on cell viability and growth. Live/dead staining (Fig. 3A) clearly illustrated cell survival on different substrates. In the control group, cells exhibited high density, well-spread morphology, and negligible red fluorescence, indicating minimal cell death. Cells cultured on PLLA and MS@Cur membranes also adhered and spread well, although slightly less extensively than those in the control group. Sparse red-stained dead cells were occasionally observed; however, quantitative analysis showed no statistically significant differences among the 3 groups (Fig. 3B, $p > 0.05$), confirming the noncytotoxic nature of both fiber types.

The CCK-8 proliferation assay (Fig. 3C) revealed comparable optical density values among all groups on day 1. With extended culture to days 3 and 5, both PLLA and MS@Cur groups exhibited proliferation trends similar to the control group, further confirming that the electrospun membranes did not impede cell growth. These findings indicate that MS@Cur provides a favorable microenvironment supporting long-term cell proliferation.

Combined with the physicochemical results, the core–shell configuration of MS@Cur effectively encapsulates curcumin within the fiber core, preventing its direct, high-concentration contact with cells. This design mitigates the potential cytostatic effects of curcumin at elevated concentrations, enabling a safe and sustained release. Consequently, MS@Cur exhibited good cytocompatibility, suggesting that its implantation at the laminectomy site didn't provoke obvious foreign-body reactions or exacerbate local inflammation, thereby creating favorable conditions for the further modulation of NETs formation within the local microenvironment.

3.3. In vitro evaluation of NETs inhibition by biomimetic patches

The formation of NETs represents a critical link between acute inflammation and chronic fibrosis.[38–40] To investigate whether the micro-sol electrospun biomimetic patch (MS@Cur) could inhibit NETs formation via curcumin sustained release, thereby interrupting the pathological activation of fibroblasts, we first employed SYTOX Green staining to visualize NETs because SYTOX Green's specific binding affinity for nucleic acids and the nucleic acid-rich structural characteristics of NETs. As shown in Figure 4A, B, the control and PLLA groups exhibited typical NETs morphology, presenting as bright green filamentous structures, whereas the MS@Cur group displayed a marked reduction in green fluorescence. SEM further revealed that neutrophils in the control and PLLA groups lost their cellular morphology and released extensive fibrous NETs networks. In contrast, most neutrophils in the MS@Cur group maintained intact cellular morphology with negligible NETs formation (Fig. 4A).

Molecular-level confirmation was provided by MPO/H3cit immunofluorescence colocalization, demonstrating that key NETs markers, MPO and H3cit,[41,42] were strongly expressed and colocalized to form mesh-like structures in the control and PLLA groups. In the MS@Cur group, both signals were significantly attenuated, as reflected in semiquantitative fluorescence analysis ($p < 0.05$) (Fig. 4C–E). Western blotting and quantification further confirmed a significant downregulation of MPO and H3cit in the MS@Cur group compared with the control and PLLA groups (Fig. 4F–H).

In the context of laminectomy, activated fibroblasts are major contributors to extracellular matrix deposition and scar formation.[43–45] NETs and their components, such as MPO and extracellular DNA, have been shown to strongly stimulate fibroblast activation, proliferation, and collagen production, perpetuating a vicious "inflammation–fibrosis" cycle.[2,13] These results indicate that

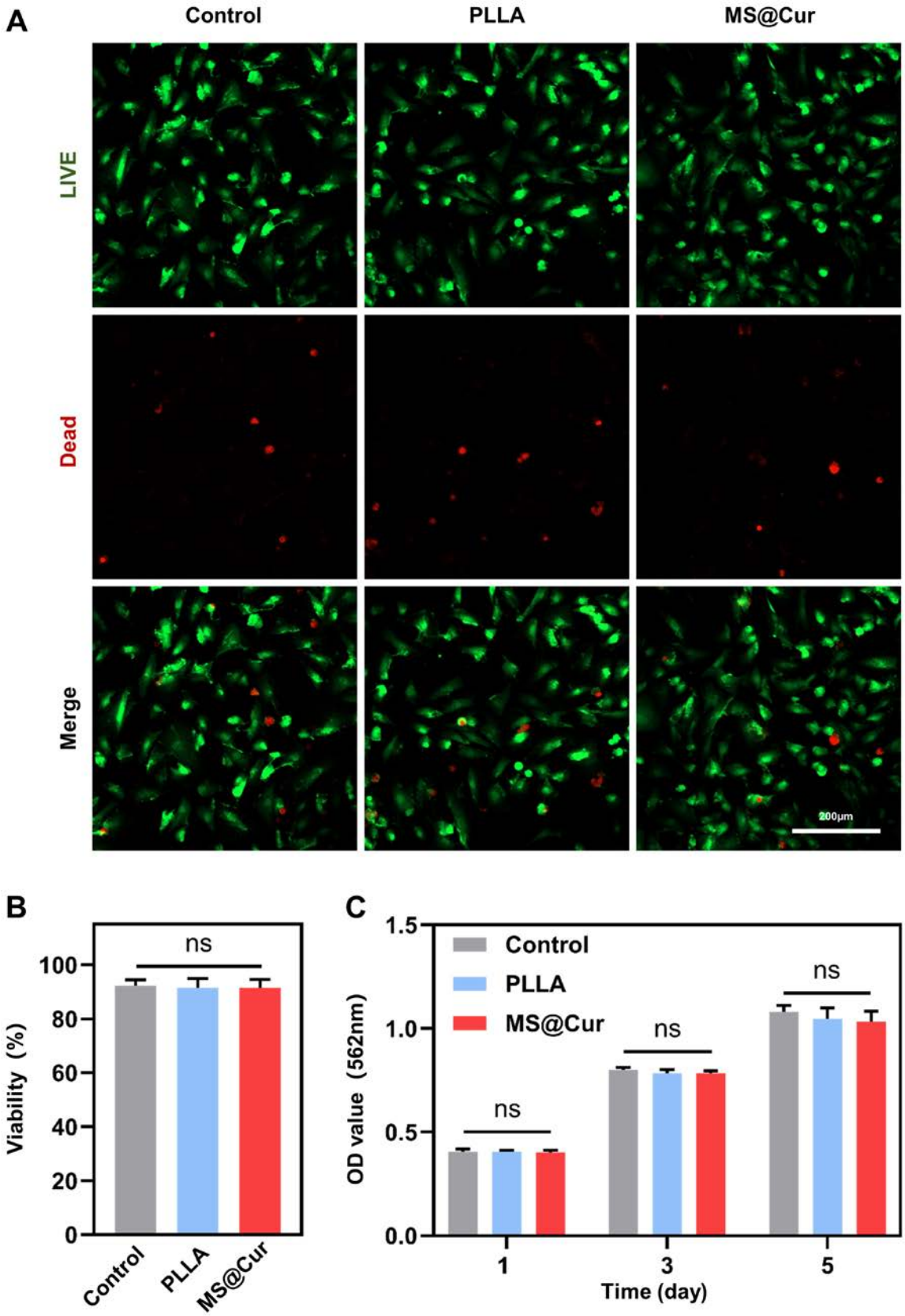

Figure 3. Evaluation of the bionic patch's biocompatibility. (A) Representative live/dead staining images showing cell viability after culture with PLLA and MS@Cur. (B) Quantification of cell viability based on live/dead staining. (C) Cell proliferation assessed by CCK-8 assay at 1, 3, and 5 days. $n = 3$, error bars, mean ± SD; all analyses were done using 1-way ANOVA with Tukey *post hoc* test, $^{*}p < 0.05$. ANOVA = analysis of variance, MS@Cur = curcumin-loaded microsol electrospun dural substitute, ns = not significant, PLLA = poly (L-lactic acid), SD = standard deviation.

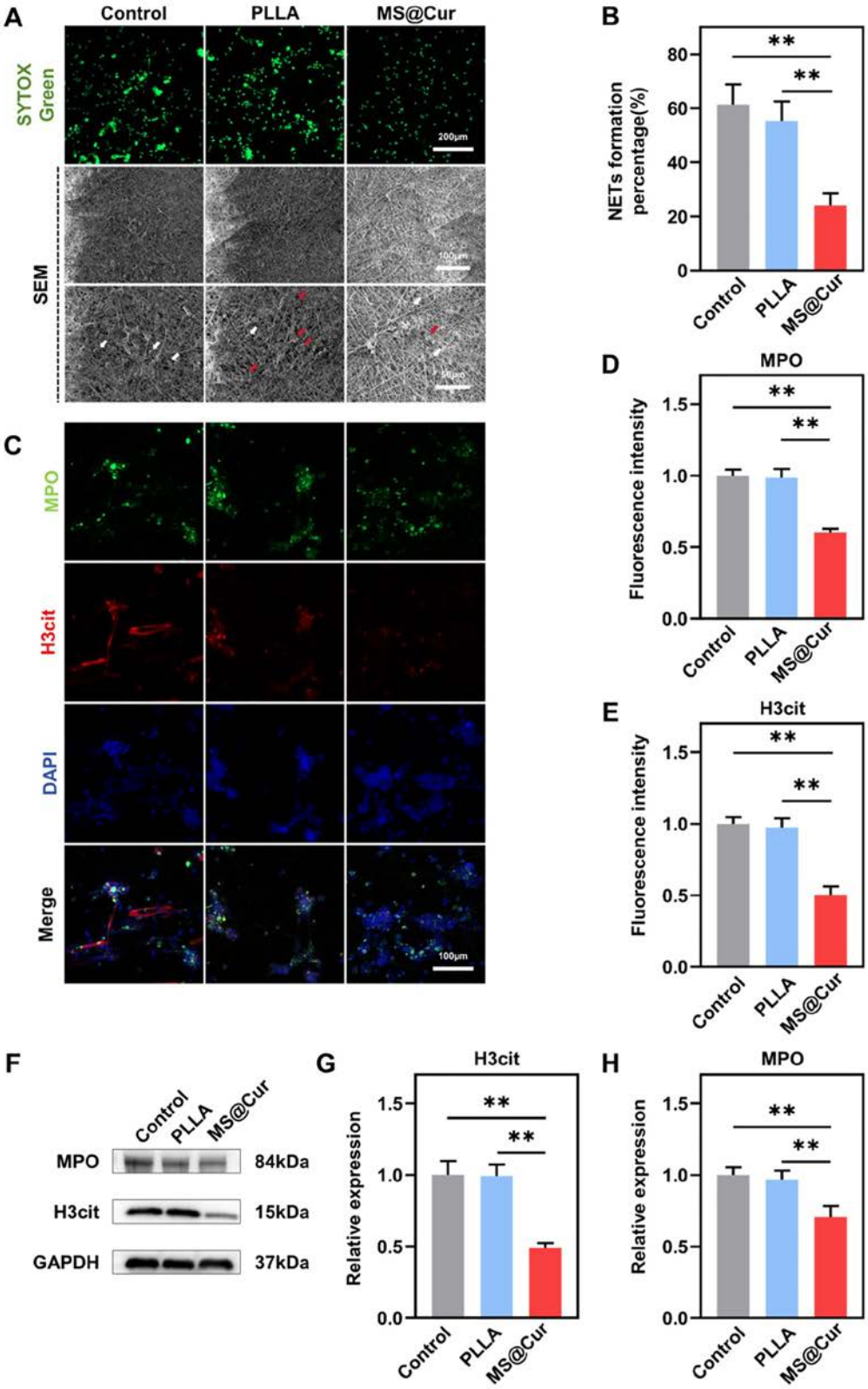

Figure 4. Evaluation of the bionic patch on NETosis inhibition. (A) Representative images of NETs visualized by SYTOX Green staining and SEM. (B) Quantitative analysis of NETs based on SYTOX Green staining. (C) Immunofluorescence staining for NETs-specific markers, myeloperoxidase (MPO, green) and citrullinated histone H3 (H3cit, red). (D, E) Semiquantitative analysis of (D) MPO and (E) H3cit fluorescence intensity. (F) Protein expression levels of MPO and H3cit detected by Western blot. (G, H) Semiquantitative analysis of (G) H3cit and (H) MPO protein expression from Western blot. $n = 3$, error bars, mean ± SD; all analyses were done using 1-way ANOVA with Tukey *post hoc* test, $^{*}p < 0.05$, $^{**}p < 0.01$. ANOVA = analysis of variance, MS@Cur = curcumin-loaded microsol electrospun dural substitute, NETs = neutrophil extracellular traps, PLLA = poly (L-lactic acid), SD = standard deviation.

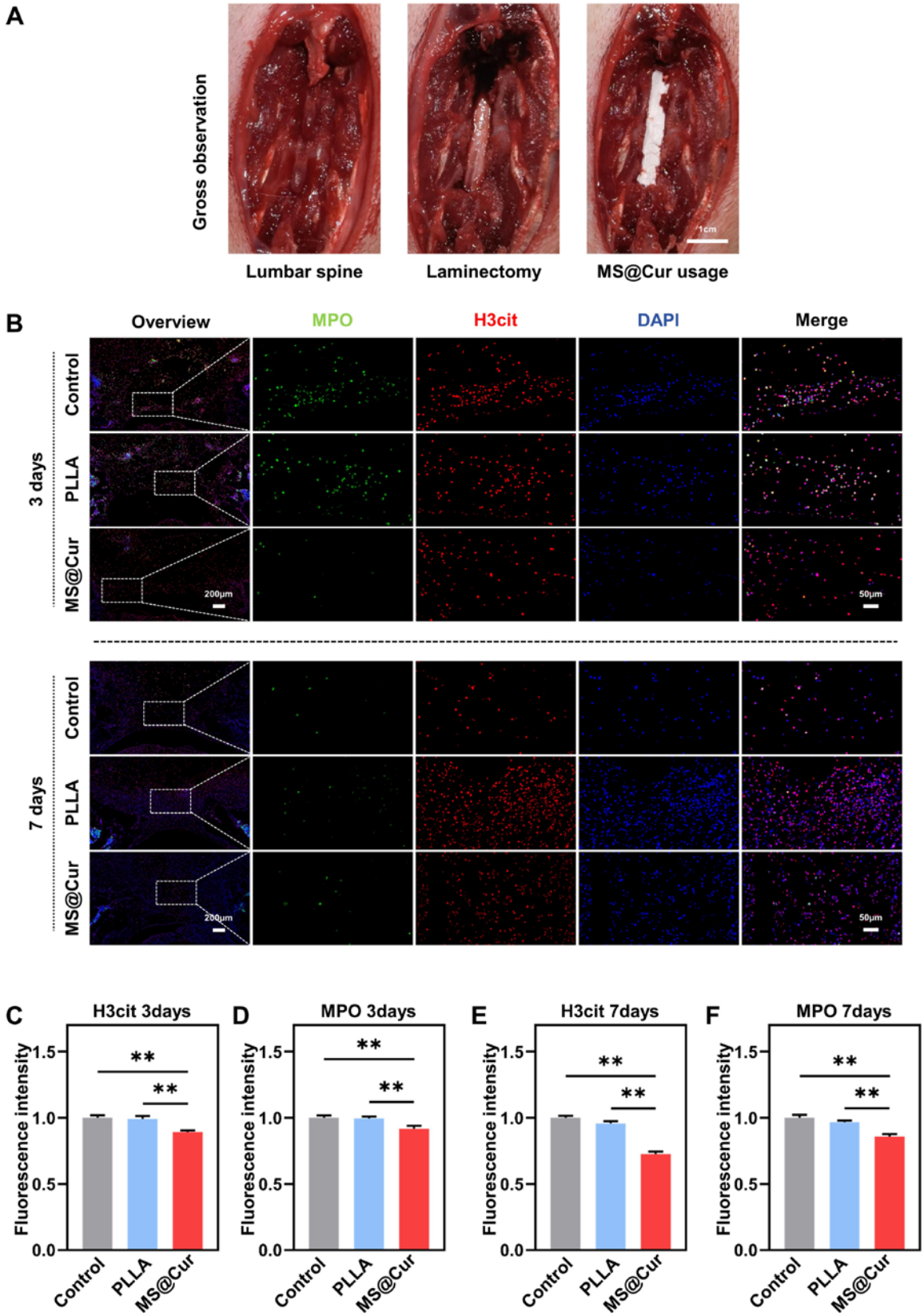

Figure 5. *In vivo* investigation of the bionic patch regulating NETs formation. (A) Schematics of the rat laminectomy model. (B) Representative immunofluorescence images of NETs-specific markers MPO (green) and H3cit (red) at postoperative days 3 and 7. (C, D) Semiquantitative analysis of fluorescence intensity for (C) H3cit and (D) MPO at day 3. (E, F) Semiquantitative analysis of fluorescence intensity for (E) H3cit and (F) MPO at day 7. $n = 3$, error bars, mean ± SD; all analyses were done using 1-way ANOVA with Tukey *post hoc* test, $^{*}p < 0.05$, $^{**}p < 0.01$. ANOVA = analysis of variance, H3cit = citrullinated histone H3, MPO = myeloperoxidase, MS@Cur = curcumin-loaded microsol electrospun dural substitute, NETs = neutrophil extracellular traps, PLLA = poly (L-lactic acid), SD = standard deviation.

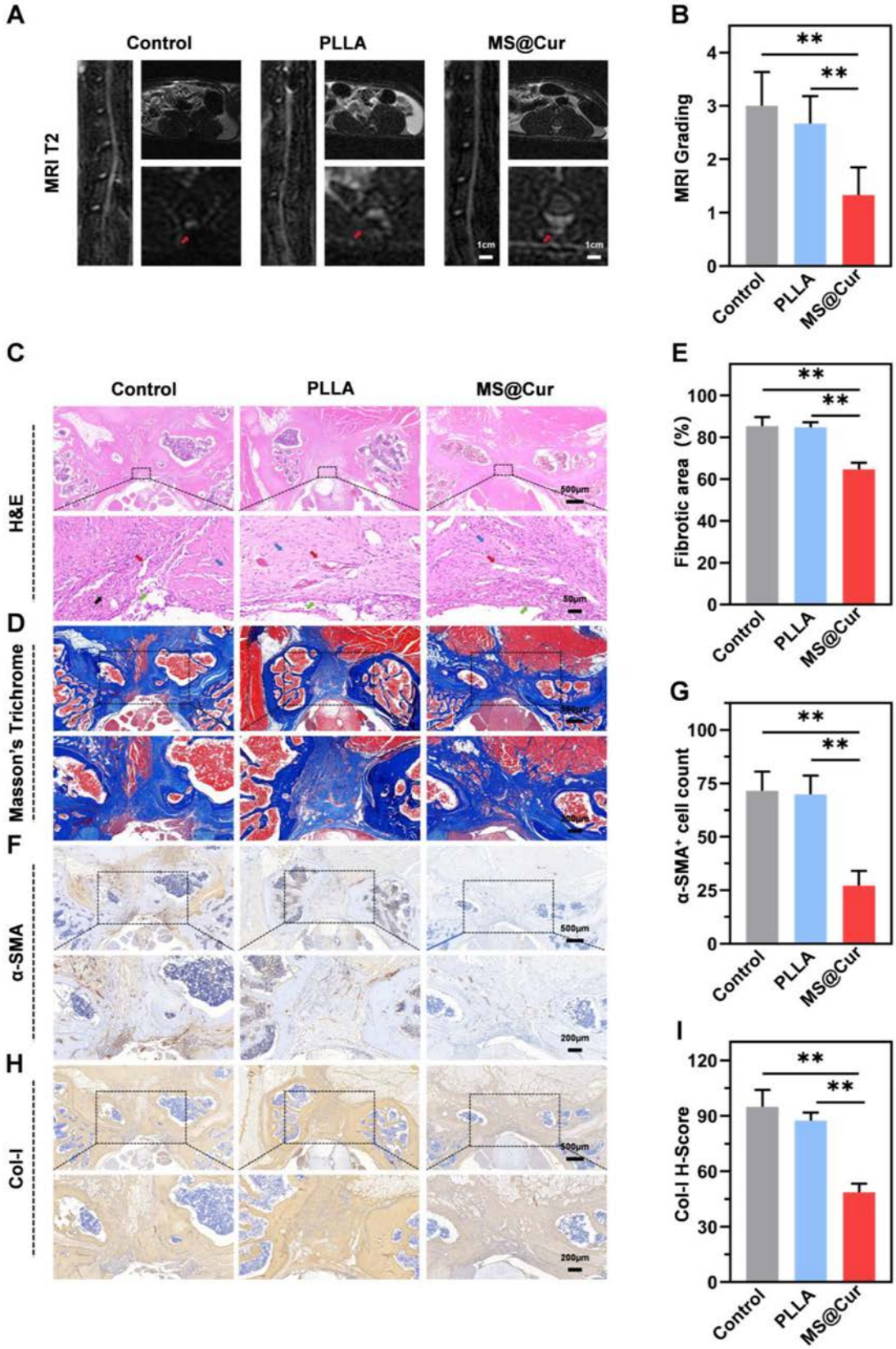

Figure 6. *In vivo* evaluation of the bionic patch for inhibiting epidural fibrosis. (A) Representative T2-weighted magnetic resonance imaging (MRI) scans at 8 weeks postoperation. (B) Semiquantitative scoring of epidural fibrosis based on MRI. (C, D) Histological analysis by (C) H&E and (D) Masson trichrome staining. (E) Semiquantitative analysis of fibrotic area. (F) Immunohistochemical (IHC) staining for fibrosis-specific markers α-SMA. (G,) Semi-quantitative analysis of IHC staining for α-SMA . (H) IHC staining for fibrosis-specific markers Collagen I (Col-I). (I) Semi-quantitative analysis of IHC staining for Col-I. $n = 3$, error bars, mean ± SD; all analyses were done using 1-way ANOVA with Tukey *post hoc* test, $^{*}p < 0.05$, $^{**}p < 0.01$. ANOVA = analysis of variance, H&E = hematoxylin–eosin, MS@Cur = curcumin-loaded microsol electrospun dural substitute, PLLA = poly (L-lactic acid), SD = standard deviation.

MS@Cur, by suppressing NETs formation, can effectively disrupt the pathological crosstalk between neutrophils and fibroblasts, mitigating early excessive inflammation and establishing a microenvironment conducive to functional repair rather than pathological scar overgrowth.

3.4. In vivo regulation of NETs and prevention of epidural fibrosis by biomimetic patches

To validate the long-term efficacy of MS@Cur in complex *in vivo* environments, we established a rat laminectomy model (Fig. 5A) and dynamically assessed NETs modulation at postoperative days 3 and 7. As shown in Figure 5B, temporal imaging revealed marked differences in NETs formation among the three groups during the early stage after laminectomy. At day 3 post-surgery, co-localization of strong MPO and H3cit positive signals were observed in the epidural region of both the Control and PLLA groups, indicating that laminectomy alone triggered a pronounced NETs response and that the conventional PLLA membrane failed to effectively prevent this process. In contrast, the MS@Cur group exhibited markedly weaker MPO and H3cit fluorescence signals, as well as substantially reduced co-localization, suggesting effective suppression of NETs formation. At day 7 post-surgery, NETs expression had decreased in all groups compared with day 3; however, the overall fluorescence intensity and co-localization area in the MS@Cur group remained notably lower than those in the Control and PLLA groups. These findings indicate that MS@Cur can continuously inhibit NETs formation in the epidural region during the early postoperative period after laminectomy. Semiquantitative fluorescence analysis further confirmed that MS@Cur effectively suppressed the formation of NETs in the epidural region after laminectomy (Fig. 5C–F).

Additionally, MS@Cur functions as a degradable physical barrier during the initial implantation phase, effectively preventing fibroblast infiltration. The sustained release of curcumin actively shapes a NETs-suppressive microenvironment. The synergistic combination of "physical isolation" and "biological modulation" underlies the long-term antiscar efficacy of MS@Cur.

To further assess the effect of NETs inhibition on late-stage epidural fibrosis, epidural scar formation was evaluated at 8 weeks postoperatively using multiple approaches. All operated rats underwent lumbar spine MRI. As shown in Figure 6A, sagittal and axial T2-weighted images revealed distinct differences in epidural tissue signals among the groups. In the Control and PLLA groups, the epidural space adjacent to the dural sac was largely occupied by extensive and heterogeneous hypointense areas, indicating severe fibrotic scar formation. In the Control group, compression of the dural sac by epidural tissue was also observed. In contrast, the MS@Cur group exhibited a relatively homogeneous epidural signal, comparable to that of the surrounding muscle tissue. The degree of fibrosis was further quantified and graded according to the MRI-based scoring system (Fig. 6B). Consistent with the imaging findings, the MS@Cur group showed significantly lower MRI grades than the Control and PLLA groups.

Histological analyses supported these findings. Hematoxylin–eosin staining (Fig. 6C) showed dense fibroblasts, abundant collagen deposition, and pronounced vascular dilation with inflammatory cell infiltration in the control group; PLLA provided structural support but inflammatory responses remained. The MS@Cur group exhibited sparse cell distribution and intact tissue architecture with markedly reduced scar tissue, demonstrating that the curcumin release system effectively restrained excessive repair and inflammatory cascades (Fig. 6E). Masson trichrome staining (Fig. 6D) further confirmed reduced collagen deposition in the MS@Cur group relative to extensive blue-stained collagen in the control and PLLA groups.

Immunohistochemistry revealed widespread α-SMA-positive myofibroblasts and a large amount of Col-I with strong positive staining in the control and PLLA groups, whereas the MS@Cur group showed significantly reduced expression (Fig 6F–I), indicating that local curcumin release reduces myofibroblast recruitment and differentiation and attenuates tissue tension and collagen cross-linking.

Collectively, these data indicate that curcumin sustained release effectively inhibits the formation of NETs, mitigating excessive collagen production and preventing epidural scar formation. Notably, transforming growth factor-β (TGF-β1) is a key factor prompting tissue fibrosis. Our research team has previously validated the participation of Smad3 signal pathway in TGF-β1-induced fibrosis.[4] However, it remains unclear whether the antifibrotic action of MS@Cur—mediated by NETs inhibition—relies on the TGF-β/Smad signaling pathway, which will be the focus of our follow-up experiments. By inhibiting NETs formation, MS@Cur was verified to effectively inhibit epidural fibrosis at laminectomy site.

4. Conclusions

In this study, we successfully developed a microsol electrospun bionic dural patch (MS@Cur) with a core–shell structure that enables sustained release of curcumin for the prevention of epidural fibrosis after laminectomy. Compared with conventional PLLA fibers, MS@Cur exhibited stable long-term drug release, thereby helping to maintain continuous local pharmacological activity. The patch also showed good cytocompatibility. *In vitro* experiments demonstrated that MS@Cur effectively inhibited the formation of NETs. *In vivo* studies further confirmed that MS@Cur significantly reduced NETs formation at early stage after laminectomy and decreased α-SMA expression and collagen deposition at later stage. Taken together, these findings suggest that the MS@Cur patch integrates the dual functions of physical isolation and biological regulation, and may represent a promising strategy for preventing epidural fibrosis by inhibiting NET formation.

Acknowledgements

None.

Ethical statement

Approval was granted by the Ethics Committee of Soochow University (SUDA20241014A16), Suzhou 215000, Jiangsu, China.

Conflicts of interest

The authors have no conflicts of interest to disclose.

Funding source

This study was supported by the National Natural Science Foundation of China (82120108017, 82272501, 82572769, 82302683), Project 333 of Jiangsu Province (2069999), the Natural Science Foundation of Jiangsu Province (BK20250123, BK20230215), Suzhou Basic Research Pilot Program: Outstanding Young Scholars Lead Project (SSD2025025), Suzhou Gusu Health Talent Program (GSWS2023093), Soochow University Medical + X project (ML12202923), and a project funded by the Priority Academic Program Development of Jiangsu Higher Education Institutions.

Data availability statement

Data collected and analyzed for the study are available from the corresponding authors upon reasonable request.

Author contributions

LC—writing original draft, conceptualization, methodology, project administration, supervision, and review and editing.
CC, KX, JT—writing original draft, methodology, project administration, formal analysis, and review and editing.
JM, FC, YG—investigation and resources.
CC, JT—software, validation, and resources.

References

[1] Alizadeh R, Sharifzadeh SR. Pathogenesis, etiology and treatment of failed back surgery syndrome. *Neurochirurgie*. 2022;68:426–31.
[2] Mei R, Sun J, Cao S, et al. Hydrogen-releasing magnesium hydrogel mitigates post laminectomy epidural fibrosis through inhibition of neutrophil extracellular traps. *Acta Biomater*. 2024;188:420–31.
[3] Echeverria-Villalobos M, Mitchell J, Fiorda-Diaz J, Weaver T. Effects of dorsal column spinal cord stimulation on neuroinflammation: revisiting molecular mechanisms and clinical outcomes on chronic lumbar/leg pain and failed back surgery syndrome. *J Pain Res*. 2021;14:2337–45.
[4] Qian M, Li S, Xi K, et al. ECM-engineered electrospun fibers with an immune cascade effect for inhibiting tissue fibrosis. *Acta Biomater*. 2023;171:308–26.
[5] Fan Q, Wu H, Kong Q. Superhydrophilic PLGA-graft-PVP/PC nanofiber membranes for the prevention of epidural adhesion. *Int J Nanomedicine*. 2022;17:1423–35.
[6] Lewik G, Lewik G, Muller LS, von Glinski A, Schulte TL, Lange T. Postoperative epidural fibrosis: challenges and opportunities - a review. *Spine Surg Relat Res*. 2024;8:133–42.
[7] Wu Q, Cui X, Guan LC, et al. Chronic pain after spine surgery: insights into pathogenesis, new treatment, and preventive therapy. *J Orthop Translat*. 2023;42:147–59.
[8] Baber Z, Erdek MA. Failed back surgery syndrome: current perspectives. *J Pain Res*. 2016;9:979–87.
[9] Brito-Garcia N, Garcia-Perez L, Kovacs FM, et al. Efficacy, effectiveness, safety, and cost-effectiveness of epidural adhesiolysis for treating failed back surgery syndrome. a systematic review. *Pain Med*. 2019;20:692–706.
[10] Wang H, Sun W, Fu D, Shen Y, Chen YY, Wang LL. Update on biomaterials for prevention of epidural adhesion after lumbar laminectomy. *J Orthop Translat*. 2018;13:41–9.
[11] Ganesh V, Kancherla Y, Igram CM, et al. Pharmacotherapies to prevent epidural fibrosis after laminectomy: a systematic review of *in vitro* and *in vivo* animal models. *Spine J*. 2023;23:1471–84.
[12] Hua F, Wang HR, Bai YF, et al. Substance P promotes epidural fibrosis via induction of type 2 macrophages. *Neural Regen Res*. 2023;18:2252–9.
[13] Jin Z, Sun J, Song Z, et al. Neutrophil extracellular traps promote scar formation in post-epidural fibrosis. *NPJ Regen Med*. 2020;5:19.
[14] Ravindran M, Khan MA, Palaniyar N. Neutrophil extracellular trap formation: physiology, pathology, and pharmacology. *Biomolecules*. 2019;9:365.
[15] Azzouz D, Palaniyar N. How do ROS induce NETosis? Oxidative DNA damage, DNA repair, and chromatin decondensation. *Biomolecules*. 2024;14:1307.
[16] Othman A, Sekheri M, Filep JG. Roles of neutrophil granule proteins in orchestrating inflammation and immunity. *FEBS J*. 2022;289:3932–53.
[17] Castanheira FVS, Kubes P. Neutrophils and NETs in modulating acute and chronic inflammation. *Blood*. 2019;133:2178–85.
[18] Wang CY, Lin TT, Hu L, et al. Neutrophil extracellular traps as a unique target in the treatment of chemotherapy-induced peripheral neuropathy. *EBioMedicine*. 2023;90:104499.
[19] Ding Q, Wei Q, Sheng G, et al. The preventive effect of decorin on epidural fibrosis and epidural adhesions after laminectomy. *Front Pharmacol*. 2021;12:774316.
[20] Kumar H, Dhalaria R, Kimta N, et al. Curcumin: a potential detoxifier against chemical and natural toxicants. *Phytother Res*. 2025;39:1494–530.
[21] Gupta SC, Prasad S, Kim JH, et al. Multitargeting by curcumin as revealed by molecular interaction studies. *Nat Prod Rep*. 2011;28:1937–55.
[22] Peng Y, Ao M, Dong B, et al. Anti-inflammatory effects of curcumin in the inflammatory diseases: status, limitations and countermeasures. *Drug Des Devel Ther*. 2021;15:4503–25.
[23] Li X, Zhu R, Jiang H, et al. Autophagy enhanced by curcumin ameliorates inflammation in atherogenesis via the TFEB-P300-BRD4 axis. *Acta Pharm Sin B*. 2022;12:2280–99.
[24] Yuan R, Li Y, Han S, et al. Fe-curcumin nanozyme-mediated reactive oxygen species scavenging and anti-inflammation for acute lung injury. *ACS Cent Sci*. 2022;8:10–21.
[25] Garodia P, Hegde M, Kunnumakkara AB, Aggarwal BB. Curcumin, inflammation, and neurological disorders: how are they linked? *Integr Med Res*. 2023;12:100968.
[26] Yang C, Zhu Q, Chen Y, et al. Review of the protective mechanism of curcumin on cardiovascular disease. *Drug Des Devel Ther*. 2024;18:165–92.
[27] Li H, Sureda A, Devkota HP, et al. Curcumin, the golden spice in treating cardiovascular diseases. *Biotechnol Adv*. 2020;38:107343.

[28] Zhu C, Shi S, Jiang P, et al. Curcumin alleviates hepatic ischemia-reperfusion injury by inhibiting neutrophil extracellular traps formation. *J Invest Surg*. 2023;36:2164813.
[29] Askarizadeh F, Karav S, Sahebkar A. Phytochemicals as modulators of NETosis: a comprehensive review on their mechanisms and therapeutic potential. *Phytother Res*. 2025;39:3545–77.
[30] Ye S, Li S, Ma Y, Hu D, Xiao F. Curcumin hinders PBDE-47-induced neutrophil extracellular traps release via Nrf2-associated ROS inhibition. *Ecotoxicol Environ Saf*. 2021;225:112779.
[31] Ma Z, Wang N, He H, Tang X. Pharmaceutical strategies of improving oral systemic bioavailability of curcumin for clinical application. *J Control Release*. 2019;316:359–80.
[32] Yan Y, Kulsoom, Sun Y, Li Y, Wang Z, Xue L, Wang F. Advancing cancer therapy: nanomaterial-based encapsulation strategies for enhanced delivery and efficacy of curcumin. *Mater Today Bio*. 2025;33:101963.
[33] Kunnumakkara AB, Harsha C, Banik K, et al. Is curcumin bioavailability a problem in humans: lessons from clinical trials. *Expert Opin Drug Metab Toxicol*. 2019;15:705–33.
[34] Wu J, Tang J, Zhang L, et al. Biomimetic "Trojan Horse" fibers modulate innate immunity cascades for nerve regeneration. *ACS Nano*. 2025;19:781–802.
[35] Fundaro SP, Salti G, Malgapo DMH, Innocenti S. The rheology and physicochemical characteristics of hyaluronic acid fillers: their clinical implications. *Int J Mol Sci*. 2022;23:10518.
[36] Raut HK, Das R, Liu Z, Liu X, Ramakrishna S. Biocompatibility of biomaterials for tissue regeneration or replacement. *Biotechnol J*. 2020;15:e2000160.
[37] Xi K, Gu Y, Tang J, et al. Microenvironment-responsive immunoregulatory electrospun fibers for promoting nerve function recovery. *Nat Commun*. 2020;11:4504.
[38] Wang H, Kim SJ, Lei Y, et al. Neutrophil extracellular traps in homeostasis and disease. *Signal Transduct Target Ther*. 2024;9:235.
[39] Wu X, Yang Y. Neutrophil extracellular traps (NETs) and fibrotic diseases. *Int Immunopharmacol*. 2024;133:112085.
[40] Li Y, Cao Z, Liu J, Qiang R, Wang J, Lyu W. Current perspectives and trends of neutrophil extracellular traps in organ fibrosis: a bibliometric and visualization study. *Front Immunol*. 2025;16:1508.
[41] Oliveira SR, de Arruda JAA, Schneider AH, et al. Neutrophil extracellular traps in rheumatoid arthritis and periodontitis: contribution of *PADI4* gene polymorphisms. *J Clin Periodontol*. 2024;51:452–63.
[42] Tan C, Aziz M, Wang P. The vitals of NETs. *J Leukoc Biol*. 2021;110:797–808.
[43] Li J, Tian J, Li C, Chen L, Zhao Y. A hydrogel spinal dural patch with potential anti-inflammatory, pain relieving and antibacterial effects. *Bioact Mater*. 2022;14:389–401.
[44] Bi X, Mao Z, Li L, et al. Janus decellularized membrane with anisotropic cell guidance and anti-adhesion silk-based coatings for spinal dural repair. *Nat Commun*. 2025;16:1674.
[45] Nie J, Sun Y, Cheng X, et al. Plant protein-peptide supramolecular polymers with reliable tissue adhesion for surgical sealing. *Adv Healthc Mater*. 2023;12:e2203301.

How to cite this article: Cui C, Xi K, Tang J, Meng J, Cai F, Gu Y, Chen L. Targeting neutrophil extracellular traps with a biomimetic patch to inhibit epidural fibrosis. *Spine Res* 2026;2(1):e00026. doi: 10.1097/br9.0000000000000026